The Earthquake-Rotated Objects Induced by the 2012 Emilia (Northern Italy) Seismic Sequence: Relation with Seismological and Geomorphological Factors

by Luigi Cucci and Andrea Tertulliani

Online Material: Table of the EROs observed following the 2012 seismic events.

INTRODUCTION

In the past few years, the awareness that earthquake-induced rotational effects can be significant in the near-fault region of an earthquake, and the consequent implications in seismic engineering, has gained rotational seismology a strong recovery in the attention of the scientific community. Impulses came from direct observations as well as numerical simulations, and special volumes related to this topic have been recently published by the *Bulletin of the Seismological Society of America* (Lee *et al.*, 2009) and by the *Journal of Seismology* (Igel *et al.*, 2012). In particular, some of the most recent papers on this subject addressed the earthquake-rotated objects (EROs hereinafter), considering the possible contribution to EROs occurrence from true rotational motion and/or translational motion (Kozák, 2006, 2009; Yang *et al.*, 2010; Hinzen, 2012), the geometry of the structure (Mucciarelli *et al.*, 2011), the clockwise/counterclockwise (CW/CCW hereinafter) sense of rotation (Yegian *et al.*, 1994), and the geological conditions at the site (Cucci and Tertulliani, 2011; Castellano *et al.*, 2012). The renewed attention to earthquake-induced rotations allowed the collection of a significant dataset of EROs following the M_w 6.3 2009 L'Aquila (Central Italy) event (see Cucci *et al.*, 2011 for a complete description of the dataset); this kind of data collection is a sound starting point for subsequent quantitative analyses of the data.

In this paper, we present a new Ⓔ dataset of EROs (available in the electronic supplement to this paper) originated by the Emilia seismic sequence, which occurred in northern Italy in 2012. The main aim of this study is to verify whether and how the distribution of the 2012 EROs is influenced by some geophysical observables (epicentral distance, intensity, directivity, lithology, etc.), in a geomorphological and seismological context completely different from that of 2009 L'Aquila.

THE 2012 EMILIA SEQUENCE

Only three years after the devastating L'Aquila earthquake, the Italian territory has been hit again by a severe damaging seismic sequence that occurred in the northern part of the country. The May–June 2012 sequence struck a broad area located in the Po Plain region, causing 26 deaths and hundreds of injured, widespread damage of historical centers and industrial areas, and an estimated economic toll of ~€2 billion. The sequence comprised two mainshocks (Fig. 1): on 20 May the first one (with M_L 5.9) occurred between Finale Emilia and S. Felice sul Panaro; on 29 May the second mainshock (with M_L 5.8) struck ~10 km southwest of the previous one. The aftershock area extends in an east–west direction for ~50 km and includes five $M_L \geq 5.0$ events and almost 2000 $M_L > 1.5$ events (ISIDe Working Group, 2010).

The seismicity distribution (Scognamiglio *et al.*, 2012), the focal mechanism of the mainshock (Pondrelli *et al.*, 2012), the Global Positioning System (GPS) and Interferometric Synthetic Aperture Radar modeling (Bignami *et al.*, 2012; Salvi *et al.*, 2012; Serpelloni *et al.*, 2012) and the distribution of the coseismic geological effects (Di Manna *et al.*, 2012; Emergeo Working Group, 2013) indicate that both mainshocks occurred on about east–west trending, south-dipping blind-thrust faults. These mechanisms are consistent with the north–south horizontal compression defined by present-day stress indicators (Montone *et al.*, 2012) and GPS-derived velocity field (Devoti *et al.*, 2011) in this region, which is characterized by buried north- and northeast-verging thrusts and folds.

The area affected by the 2012 sequence is characterized by low instrumental seismicity (Castello *et al.*, 2006; ISIDe Working Group, 2010) and rather infrequent strong historical events (Rovida *et al.*, 2011; Castelli *et al.*, 2012), with a consequent low level of seismic classification. The macroseismic survey of the 2012 events showed that the maximum intensity reached EMS98 = 8 and that the largest damage was distributed in an east–west direction (Galli *et al.*, 2012; Tertulliani *et al.*, 2012).

doi: 10.1785/0220130046

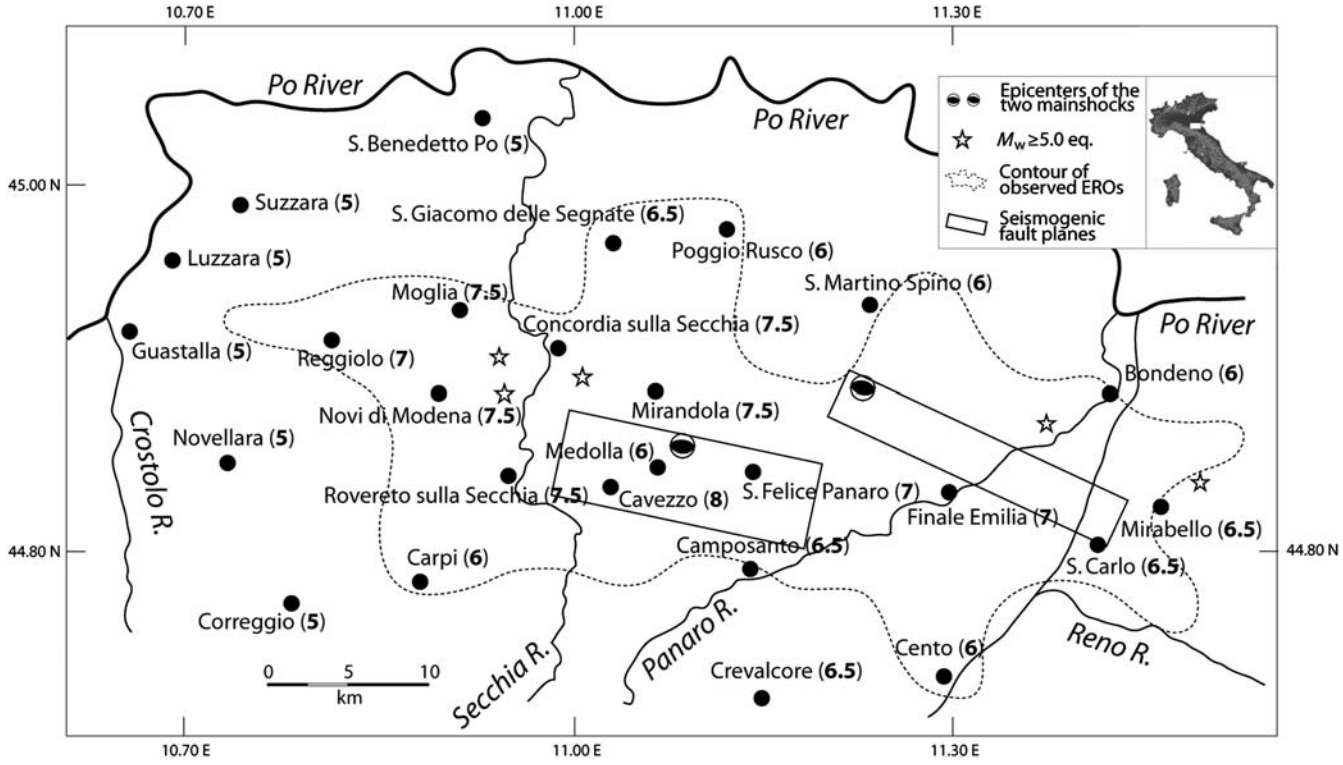

▲ **Figure 1.** Map of the study area. The focal mechanisms by Scognamiglio *et al.* (2012) indicate the position of the epicenters of the 20 and 29 May mainshocks. $M_L \geq 5.0$ earthquakes between 20 May and 20 August from ISIDe, the Italian Seismic Instrumental and Parametric Data-basE (http://iside.rm.ingv.it/iside/standard/index.jsp, last accessed September 2013). A dashed curved line encircles the area where earthquake-induced rotational effects have been observed. We also show the surface projection of the seismogenic sources by Bignami *et al.* (2012) and the main localities in the study area along with their EMS-98 intensity (Galli *et al.*, 2012; Tertulliani *et al.*, 2012).

A general increase in the damage severity and a westward shift in the major damage area were observed following the 29 May M_L 5.8 earthquake, that was characterized by a remarkable 0.9*g* vertical component of ground motion (Dolce *et al.*, 2012). No significant directivity in the earthquake effects was observed, though Piccinini *et al.* (2012) report that a great part of the energy during the 20 May event was radiated by a source propagating toward the west-southwest.

MAP OF THE EARTHQUAKE-ROTATED OBJECTS

Many rotated objects were observed during the macroseismic survey carried out in the aftermath of the 20 May and 29 May mainshocks (Fig. 2). The observations include many manufactured objects that have rotated entirely or partially. The Ⓔ dataset (see supplement) consists of chimneys, columns, pillars, statues, capitals, both free-field-based (i.e., resting directly on the ground, FFD hereinafter) and building-based (BDG); whereas FFD objects can be considered as potential indicator of pure rotational ground motion, BDG objects could have been affected by rotational modes of the underlying structure (Cucci and Tertulliani, 2011). Our database counts 94 observations (16 FFD and 78 BDG) at 35 different locations (Fig. 2), mostly concentrated in the epicentral area. As usual, the most frequently rotated object is the chimney (built of concrete blocks, bricks, or flues) that is observed spun in its body or in the top only. In several instances, the rotation affected pillars or capitals on walls and gates.

A first general look at the distribution of the EROs (Figs. 1 and 2) shows that the rotations are mainly concentrated at localities where the observed macroseismic intensities are within a range of 6–7 and 7–8 (Galli *et al.*, 2012; Tertulliani *et al.*, 2012). Also, the area where earthquake-induced rotational effects have been observed resembles (although slightly wider) the general pattern of highest damage, and appears equally distributed with respect to the azimuth to the epicenters of the two mainshocks.

EROS DISTRIBUTION AND SEISMOLOGICAL OBSERVABLES

The most important characteristics of the 2012 sequence lie in its double mainshock and in the faulting mechanism; therefore, we will now focus on these seismological factors and evaluate possible correlations with our EROs dataset.

Because of the short time span between both mainshocks and the corresponding field surveys, we were able to distinguish most of observed effects between the two earthquakes, even in those localities that were equally affected by both the events. Figure 3 shows plots of the EROs distribution in relation to the

▲ **Figure 2.** Map of the observation sites of rotational effects and examples of rotations. The numbers inside the green circles indicate multiple observations associated to the same site. The focal mechanisms indicate the epicenters of the 2012 mainshocks. The numbers in the lower right corner of each photo indicate the corresponding record in the ⊠ electronic supplement to this paper. The gray shaded area represents the area of maximum damage (Int ≥6.5).

seismicity subsequent to each mainshock. We find several similarities between these distributions that can be summarized as follows:

- *EROs locations do not correlate with the aftershock cloud*. This is especially valid for the 56 EROs observed after the 20 May shock (Fig. 3a), which simply juxtapose to seismicity, and slightly less straightforward for the 38 EROs caused by the 29 May event (Fig. 3b).
- *EROs are unevenly distributed with respect to the strike of the seismogenic source*. In both cases, a remarkable number of EROs, exceeding 50% of the total (29 out of 56 for the first mainshock, 20 out of 38 for the second), are located west of the responsible fault planes, whereas a small number (one and five, respectively) are east.
- Except for one single rotation observed on 29 May south of Medolla, no ERO falls within the surface projection of the seismogenic source.
- *In both cases, more than 90% of EROs are located on the hanging wall of the fault*. The possible explanations of this pattern in terms of seismological parameters (faulting mechanism and geometry of the source) will be addressed in the following; at this stage, we want to point out that this pattern cannot be ascribed to variations in the settlement consistency in the area across the two sides of the faults.
- *The absolute majority of the EROs was observed in the near-field zone*, with more than 90% of the sites within a distance of one fault length. The average epicentral distance is 12.4 km ($\sigma = 3.9$ km) for the EROs induced by the 20 May event and 15.1 km ($\sigma = 7.8$ km) for those induced by the 29 May event. This last observation is not straightforward as the higher average distance is associated with the less energetic earthquake. However, such values of distance are fully comparable with those recorded following the L'Aquila earthquake (≈12 km; Cucci and Tertulliani, 2011).
- *A particular feature of the EROs is the CW/CCW sense of rotation*. We observe that the CW/CCW distribution of

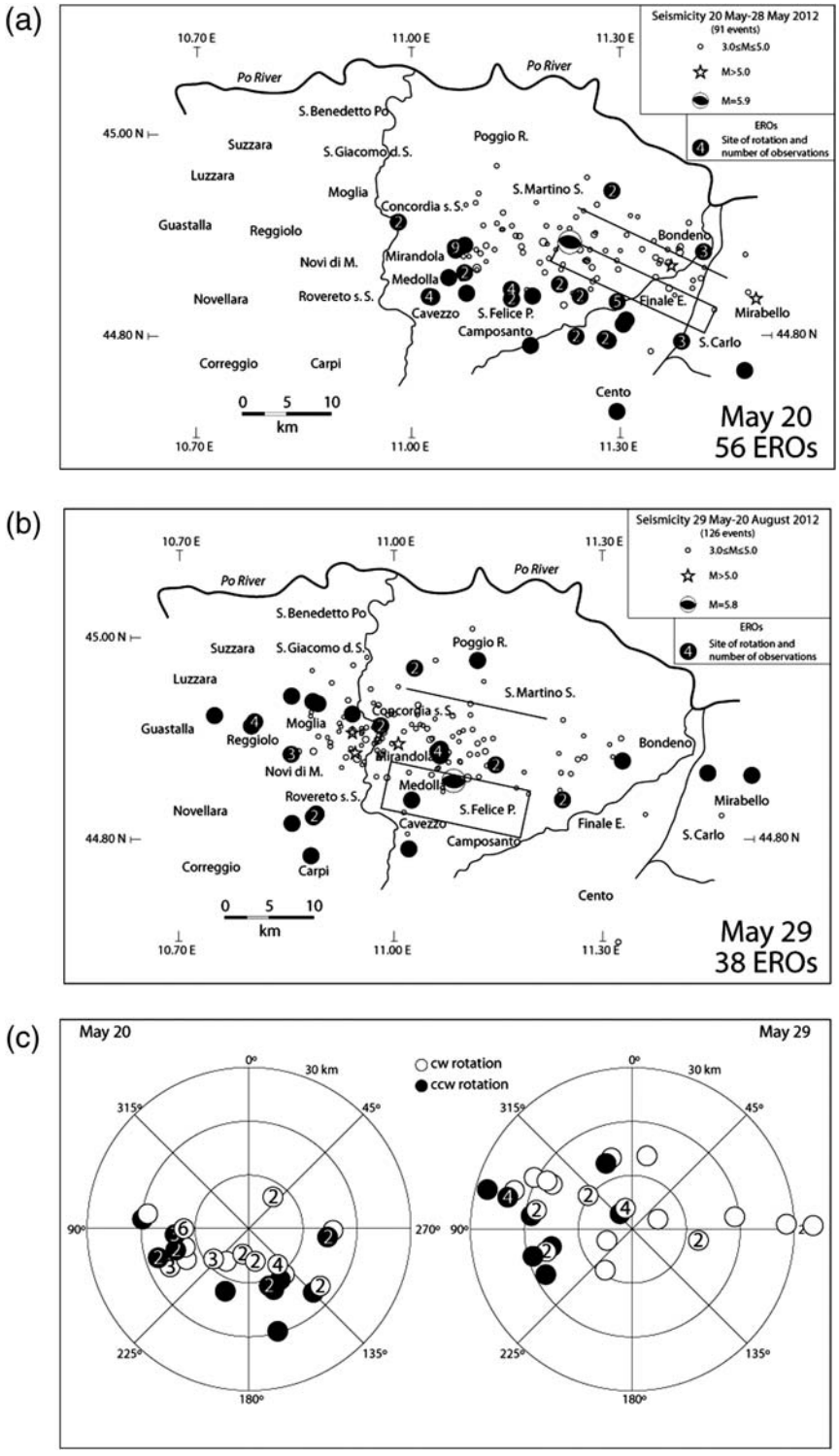

▲ **Figure 3.** Distribution of the EROs and seismicity. (a) EROs induced by the 20 May event and seismicity in the period 20–28 May. White numbers inside circles, multiple observations associated with the same site; the focal mechanism marks the epicenter of the first mainshock. We also show the surface vertical projection of the seismogenic source and its probable intersection with the surface. (b) EROs induced by the 29 May event and seismicity in the period 29 May–20 August. White numbers inside circles, multiple observations associated with the same site. The focal mechanism marks the epicenter of the second mainshock. We also show the surface vertical projection of the seismogenic source and its probable intersection with the surface. (c) Polar plots of the distribution of the sense of rotation after the two mainshocks. Open and filled circles, clockwise and counterclockwise rotation of ERO; the angle corresponds to the azimuth and the radial axis (values at the outer circle in the north-northeast) to the epicentral distance. Numbers inside circles, multiple observations associated with the same site.

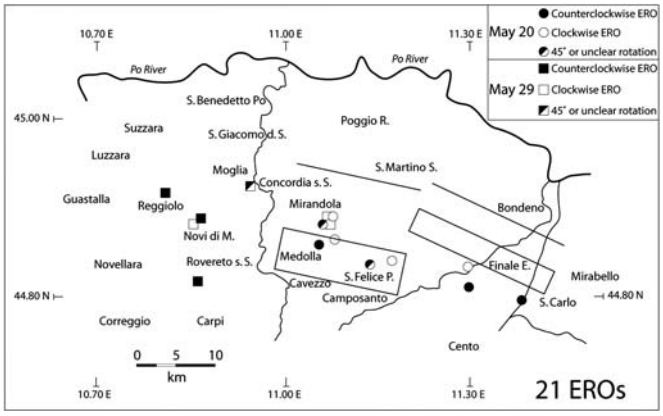

▲ **Figure 4.** Map of the distribution of the free-field-based (FFD) EROs. Circles, EROs induced by the 20 May event; squares, EROs induced by the 29 May event; open symbols, clockwise rotations; filled symbols, counterclockwise rotations. We also show the surface vertical projection of the seismogenic source and its probable intersection with the surface.

the EROs caused by the 2012 sequence (Fig. 3c) follows a peculiar pattern. For both mainshocks, CCW rotations appear more clustered (south of the epicenter of 20 May and west of the epicenter of 29 May, respectively) than the CW ones are. Furthermore, CCW rotations display a significantly higher average epicentral distance than CW rotations (14.0 km/σ = 2.8 km versus 11.7 km/σ = 3.9 km on 20 May, 19.1 km/σ = 6.3 km versus 14.2 km/σ = 7.9 km on 29 May; see Fig. 3c).

- *Finally, if we focus our analyses on the FFD objects only, we observe that this particular subset of data is distributed along a very narrow west-northwest–east-southeast-trending strip of territory* (Fig. 4) that follows the mean strike of the seismogenic faults and coincides with the highest damage area. FFD data display average epicentral distances that resemble those of the entire dataset (11.5 km for 20 May, 14.3 km for 29 May), and again the higher distance is associated with the smaller earthquake.

EROS DISTRIBUTION AND GEOMORPHOLOGICAL FACTORS

The particular geological setting at a site, that is, outcropping lithology and local amplification factor, was found to be the most significant contributor to EROs occurrence following the L'Aquila event, which affected a small intramountain basin within the Apennines thrust and fold mountain belt. However, the location of the 2012 earthquakes is completely different, as they are placed in the midst of the flat Po alluvial plain. Hence, the area is characterized by almost total absence of topographic contrast and by uniform surface lithologies consisting of Holocene alluvial deposits (mostly silts and clays) originated by the Po River and its flood waters.

In this environment, almost all sites are prone to potential amplification of the seismic shaking (http://ambiente.regione.emilia-romagna.it/geologia/temi/sismica/, last accessed September 2013). The only geomorphologically distinctive factor at the surface in this rather monotonous landscape is actually provided by the rivers and by their evolution through time. A number of abandoned river beds, paleo-levee ridges and artificial channels testify of historical episodes of flooding and/or course deflections of the Secchia, Panaro, and Reno rivers, and of the following attempt of reclaim by man. These geomorphological features, mainly formed by saturated sands, hosted a great number of liquefaction effects during the 2012 seismic sequence (Di Manna *et al.*, 2012; Emergeo Working Group, 2013). Because of their origin, most of these features are slightly higher (2–4 m) than the basal level of the plain and represent a preferential location for human settlement.

To assess whether the distribution of the observed rotations can be correlated with these features, we superimpose our data on the geomorphological map by Castiglioni *et al.* (1999), who carefully mapped paleo riverbeds and levee ridges in the study area. Noticeably, we observe that more than three quarters of the rotations appear concentrated and aligned along the paleomorphologies (Fig. 5). In particular, more than 60% of the total EROs (57 out of 94) are located in correspondence to paleo-levee ridges more or less pronounced and elevated on the ground level of the plain, and another 14 EROs are observed along medium- to well-preserved paleo riverbeds. The remaining 23 EROs (24.5% of the total) were located well outside abandoned riverbeds and ancient levee ridges. As for the FFD objects, we observe that the distribution of this particular kind of EROs does not deflect from that of the whole dataset, as about two thirds of the rotations were located in correspondence to paleo riverbeds. Similarly, we did not observe significant variations in the percentage of EROs occurrence on those paleomorphologies depending on the two different mainshocks or on the CW/CCW sense of rotation.

One might wonder whether the remarkable correspondence between location of the EROs and geomorphological features could be directly ascribed to the tendency to settle residential areas on levee ridges and paleo riverbeds. Actually, in the ~2750 km^2 wide study area we note that the total built-up surface extends over ~156 km^2, and that only 55 km^2 (equal to 35% of the residential areas) are settled on paleo riverbeds. Thus, dense housing on particular geomorphological features only partially accounts for EROs occurrence. Another subsurface geomorphological factor to take into account is the presence of a buried morphological structure with a strongly varying depth, such as the folded sequence underlying the Holocene continental deposits. Around Mirandola, where most of the EROs are observed (Fig. 5), the top of this structure is very shallow (50–100 m.b.s.l.) and is aligned along a west-northwest–east-southeast direction (Boccaletti and Martelli, 2004). Moving northward and southward the boundary of the structure dips to several hundreds of meters and EROs rarefy (Fig. 5). Consequently, strong lateral variations of shear-wave velocity in the north–south direction might also affect the fundamental soil frequency in the area (e.g., Priolo

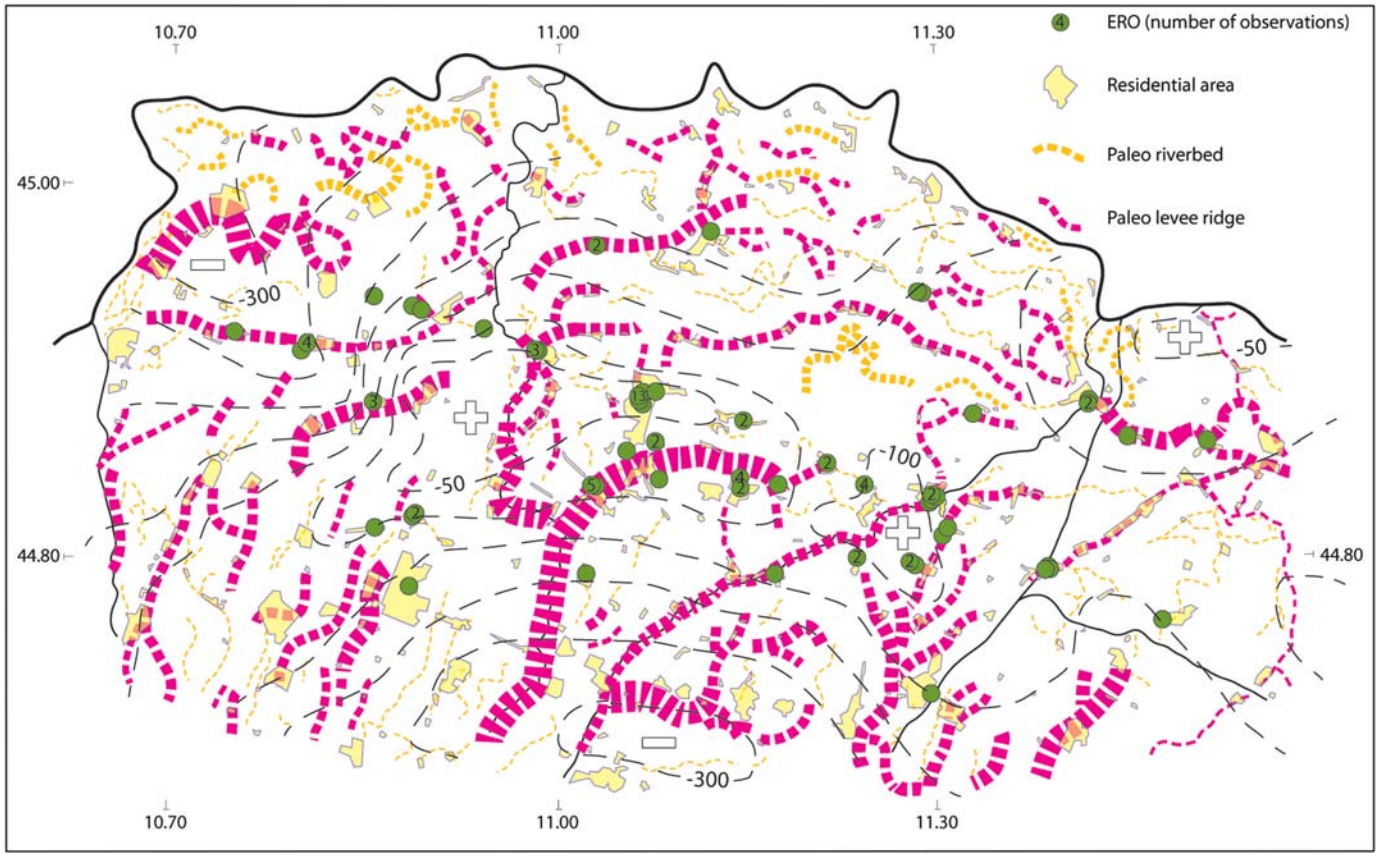

▲ **Figure 5.** Distribution of the EROs, village boundaries and geomorphological features in the area. Circles, EROs induced during the sequence (numbers mark multiple observations associated to the same site); red dashed heavy lines, levee ridges; ochre dashed lines, poorly to well-preserved paleo riverbeds; black dashed thin lines, contour depth of the top of the upper–mid-Pleistocene marine deposits in the area (Boccaletti and Martelli, 2004); light-yellow polygons, residential areas.

et al., 2012), providing a plausible explanation of the pattern of EROs distribution.

DISCUSSION

The 2012 Emilia earthquakes produced an impressive number of EROs throughout a wide area of the Po Plain (see Ⓔ supplement). As the consistency of the 2012 dataset was comparable with that produced by the 2009 L'Aquila event, an important issue was to verify which factors could be significant contributors to EROs occurrence in such different geomorphological (intramountain basin versus alluvial plain) and seismological (normal versus thrust faulting) environments.

The analysis of the 2012 EROs provides a series of distinctive features that indicate similarities between the two datasets from a seismological perspective. Indeed, most of the observations distribute in the near-field zone, with more than 90% of the EROs located within a distance of one fault length and average epicentral distances ranging 12–15 km. Moreover, even in 2012 the rotations are mainly concentrated in areas of intermediate damage (EMS98 intensity between 6 and 7), with only one third of the EROs observed in localities marked by the highest intensities (7–8 and 8). Therefore, a first significant conclusion that is in common between the 2009 and 2012 events is that there is a clear convergence between rotations and damage, as the general distribution of the EROs resembles that of the intensities.

However, there are also clear differences between the distribution of the EROs induced by the 2009 and 2012 sequences, such as: (1) the sharp separation between EROs and seismicity, (2) the almost total absence of rotations within the surface projection of the two blind seismogenic sources in 2012, (3) the higher average distance of the EROs induced by the less energetic 29 May M_L 5.8 mainshock, (4) the small effects of directivity, and (5) the overwhelming (more than 90%) occurrence of EROs on hanging walls. We suggest that these differences are related to the geometry of the source and the faulting mechanism. As a matter of fact, empirical evidence, lab experiments, and field observations show the occurrence of stronger near-source ground motion from thrust faults than from normal faults and higher ground motion on the hanging wall than on the footwall (Oglesby *et al.*, 2000a,b; Aochi and Olsen, 2004; Chang *et al.*, 2004). Furthermore, hanging-wall sites exhibit high acceleration at greater distances from the source than footwall sites (Chang *et al.*, 2004). Although such effects can be less energetic when applied to blind thrusts

(Oglesby *et al.*, 2000a), and considering that purely translational ground motions are sufficient to induce vertical rotation (Hinzen, 2012), we believe that such combination of geometry and kinematics observations may explain the points listed above with the exception of point (4) (unusual average distance). For this latter point we suppose that the more widespread EROs distribution induced on 29 May might be related to the lower angle of dip of the seismogenic fault (20° versus 43°; Bignami *et al.*, 2012), and/or to the very large vertical component of ground motion caused by the second mainshock.

As for the distribution of the CW/CCW sense of rotation, caution has to be paid because CW and/or CCW EROs were sometimes observed randomly distributed following past earthquakes (see Hinzen, 2012; and references therein), and because the predictability of this observable at a given site is debated (Castellano *et al.*, 2012). However, among the studies that addressed this issue, Hinzen (2012) found that phase differences in the horizontal ground motion can influence the sense of rotation at a given site, whereas Bouchon and Aki (1982) observed that (for a strike-slip fault) the change of residual rotation from a sense to another occurs at a distance that depends on the depth to the top of the fault. As both these indications basically imply a relation between sense of rotation and epicentral distance, we deduce (though only qualitatively) that the particular clustering and the different average epicentral distance between CW and CCW rotations exhibited following both the 2012 mainshocks depend on the distance from the source.

Finally, if we focus on the FFD objects, which can potentially represent true rotational ground motion, we find that the distribution of FFD EROs emphasizes the tight relation between rotations and damage already displayed by the whole dataset, and highlights the influence of the dip of the source on the total extent of the area affected by EROs occurrence.

The comparison between EROs observed in 2012 and geological data certainly confirms the indication, first put into evidence by Cucci and Tertulliani (2011) and Castellano *et al.* (2012) after the L'Aquila earthquake, that the rotational motion can be greatly enhanced by the specific geological setting at a site, as well as by the potential amplification of the ground motion. Although the Po Plain area is characterized by uniform surface lithology and negligible topography, the great majority of EROs in 2012 occurred along particular geomorphological structures of limited extent, such as paleo riverbeds and levee ridges. These structures are usually made of reclaimed land and/or reworked material and can contain saturated sands, and ultimately are affected by scarce geophysical and/or geotechnical characteristics (Athanasopoulos-Zekkos and Saadi, 2012). As for the amplification of ground shaking as contributor to local rotations, we observe that in the 2012 case this characteristic affects all the sites with no exception. Therefore, we suggest that the amplification factor due to the local geological condition did not play a prominent role in inducing rotational motion at any given site; rather it represents the main trigger for EROs occurrence in the area as a whole. In this sense, a possible contribution to EROs distribution could be provided by lateral variations of shear-wave velocity associated with morphological structures buried at different depths. These considerations would also account for the unusual wealth of data if one considers the relatively low magnitude of the earthquakes that produced the 2012 dataset. Conversely, the almost total absence of topographic contrast in the study area is an indirect confirmation of the indication that ground rotations are not strongly dependent on the topography, as also suggested by Castellano *et al.* (2012) with examples in downtown L'Aquila at a more detailed scale. No remarkable variations in our results are observed if we restrict our analyses to the relationships between FFD EROs, CW/CCW partition, and geomorphology. In other words, once a seismic event has occurred, the geomorphological characteristics represent a sort of first order constraint to the general occurrence of earthquake-rotated objects.

CONCLUSIONS

The main conclusions of the analyses performed in this study can be listed as follows:

1. There is a significant overlap of EROs distribution and damage;
2. three quarters of EROs occur on paleo riverbeds and levee ridges affected by the most extreme geophysical–geotechnical characteristics throughout the area;
3. more than 90% of EROs occur on the hanging walls;
4. the CW/CCW partition might depend on the distance from the source;
5. faulting mechanism, dip of the source, and distance from the fault can influence the total extent of the area affected by EROs occurrence and, in particular, the distribution of those EROs that more probably reflect true rotational motion.

In summary, this study confirms the importance of the combination of geomorphological factors and amplification of the seismic motion as the leading factors influencing the occurrence and the nature of the earthquake-induced rotational effects. However, the presence of anomalies and/or of particular patterns in the EROs distribution can be caused by seismological factors, among which we cite the faulting mechanism and the geometry of the source.

We believe that this kind of study is a fundamental input for quantitative evaluations of earthquake-induced rotations in the near field and is a precondition for earthquake engineering analyses like those following the L'Aquila event (Hinzen *et al.*, 2013).

ACKNOWLEDGMENTS

We thank the associate editor and two anonymous reviewers for constructive suggestions and comments that improved the paper. F. R. Cinti and Klaus-G. Hinzen read and corrected a first draft of the manuscript; we thank them for valuable discussions and important suggestions. B. Angioni and

E. Rocchetti provided support for the production of the electronic supplement.

REFERENCES

Aochi, H., and K. B. Olsen (2004). On the effects of nonplanar geometry for blind thrust faults on strong ground motion, *Pure Appl. Geophys.* **161,** 2139–2153, doi: 10.1007/s00024-004-2554-x.

Athanasopoulos-Zekkos, A., and M. Saadi (2012). Ground motion selection for liquefaction evaluation analysis of earthen levees, *Earthq. Spectra* **28,** 1331–1351.

Bignami, C., P. Burrato, V. Cannelli, M. Chini, E. Falcucci, A. Ferretti, S. Gori, C. Kyriakopoulos, D. Melini, M. Moro, F. Novali, M. Saroli, S. Stramondo, G. Valensise, and P. Vannoli (2012). Coseismic deformation pattern of the Emilia 2012 seismic sequence imaged by Radarsat-1 interferometry, *Ann. Geophys.* **55,** no. 4, doi: 10.4401/ag-6157.

Boccaletti, M., and L. Martelli (Editors) (2004). *Carta sismotettonica della Regione Emilia-Romagna, Firenze*, S.E.L.C.A., 60 pp. (in Italian).

Bouchon, M., and K. Aki (1982). Strain, tilt, and rotation associated with strong ground motion in the vicinity of earthquake faults, *Bull. Seismol. Soc. Am.* **72,** 1717–1738.

Castellano, C., L. Cucci, A. Tertulliani, and G. Pietrantonio (2012). Rotational effects associated with ground motion during the M_w 6.3 2009 L'Aquila (Central Italy) earthquake, *Bollettino di Geofisica Teorica ed Applicata* **53,** 299–312, doi: 10.4430/bgta0045.

Castelli, V., F. Bernardini, R. Camassi, C. H. Caracciolo, E. Ercolani, and L. Postpischl (2012). Looking for missing earthquake traces in the Ferrara-Modena plain: An update on historical seismicity, *Ann. Geophys.* **55,** no. 4, 519–524, doi: 10.4401/ag-6110.

Castello, B., G. Selvaggi, C. Chiarabba, and A. Amato (2006). CSI Catalogo della Sismicità Italiana 1981–2002, versione 1.1. INGV-CNT, Roma; http://csi.rm.ingv.it, last accessed September 2013 (in Italian).

Castiglioni, G. B., A. Biancotti, M. Bondesan, G. C. Cortemiglia, C. Elmi, V. Favero, G. Gasperi, G. Marchetti, G. Orombelli, G. B. Pellegrini, and C. Tellini (1999). Geomorphologic map of the Po Plain, Italy, at a scale of 1:250000, *Earth Surf. Proc. Land.* **24,** 1115–1120, doi: 10.1002/(SICI)1096-9837(199911)24:12<1115::AID-ESP38>3.0.CO;2-Z.

Chang, T.-Y., F. Cotton, Y.-B. Tsai, and J. Angelier (2004). Quantification of hanging-wall effects on ground motion: Some insights from the 1999 Chi-Chi earthquake, *Bull. Seismol. Soc. Am.* **94,** no. 6, 2186–2197.

Cucci, L., and A. Tertulliani (2011). Clues for a relation between rotational effects induced by the M_w 6.3 2009 L'Aquila (Central Italy) earthquake and site and source effects, *Bull. Seismol. Soc. Am.* **101,** 1109–1120.

Cucci, L., A. Tertulliani, and C. Castellano (2011). The photographic dataset of the rotational effects produced by the 2009 L'Aquila earthquake, *Miscellanea INGV* **11,** 62 pp.

Devoti, R., A. Esposito, G. Pietrantonio, A. R. Pisani, and F. Riguzzi (2011). Evidence of large-scale deformation patterns from GPS data in the Italian subduction boundary, *Earth Planet. Sci. Lett.* **311,** 230–241, doi: 10.1016/j.epsl.2011.09.034.

Di Manna, P., L. Guerrieri, L. Piccardi, E. Vittori, D. Castaldini, A. Berlusconi, L. Bonadeo, V. Comerci, F. Ferrario, R. Gambillara, F. Livio, M. Lucarini, and A. Michetti (2012). Ground effects induced by the 2012 seismic sequence in Emilia: Implications for seismic hazard assessment in the Po Plain, *Ann. Geophys.* **55,** no. 4, doi: 10.4401/ag-6143.

Dolce, M., M. Nicoletti, A. Ammirati, R. Bianconi, L. Filippi, A. Gorini, S. Marcucci, F. Palma, E. Zambonelli, G. Lavecchia, R. de Nardis, F. Brozzetti, P. Boncio, D. Cirillo, A. Romano, G. Costa, A. Gallo, L. Tiberi, G. Zoppé, P. Suhadolc, F. Ponziani, and A. Formica (2012). *The Ferrara Arc Thrust Earthquakes of May–June 2012 (Northern Italy): Strong-Motion and Geological Observations*, Report II, National Civil Protection Department (DPC), http://www.protezionecivile.gov.it/jcms/it/ran.wp (last accessed September 2013).

Emergeo Working Group (2013). Liquefaction phenomena associated with the Emilia earthquake sequence of May–June 2012 (Northern Italy), *Nat. Hazards Earth Syst. Sci.* **13,** 935–947, doi: 10.5194/nhess-13-935-2013.

Galli, P., S. Castenetto, and E. Peronace (2012). May 2012 Emilia earthquakes (M_w 6, northern Italy): Macroseismic effects distribution and seismotectonic implications, *Alp. Mediterr. Quat.* **25,** 105–123 (in press), available online at http:/amq.aiqua.it (last accessed September 2013).

Hinzen, K.-G. (2012). Rotation of vertically oriented objects during earthquakes, *J. Seismol.* **16,** 797–814, doi: 10.1007/s10950-011-9255-6.

Hinzen, K.-G., L. Cucci, and A. Tertulliani (2013). Rotation of objects during the 2009 L'Aquila earthquake analyzed with 3D laserscans and discrete element models, *Seismol. Res. Lett.* **84,** doi: 10.1785/0220130010.

Igel, H., J. Brokesova, J. Evans, and Z. Zembaty (Guest Editors) (2012). Advances in rotational seismology: Instrumentation, theory, observations, and engineering, *J. Seismol.* **16,** 571–838.

ISIDe Working Group (2010). *Italian Seismological Instrumental and Parametric Database*, http://iside.rm.ingv.it (last accessed September 2013).

Kozák, J. T. (2006). Development of earthquake rotational effect study, in *Earthquake Source Asymmetry, Structural Media and Rotation Effects*, R. Teisseryre, R. M. Takeo, and E. Melijewski (Editors), Springer Verlag, Berlin and Heidelberg, 3–10.

Kozák, J. T. (2009). Tutorial on earthquake rotational effects: Historical examples, *Bull. Seismol. Soc. Am.* **99,** 998–1010.

Lee, W. H. K., M. Celebi, M. I. Todorovska, and H. Igel (Guest Editors) (2009). Special issue on rotational seismology and engineering applications, *Bull. Seismol. Soc. Am.* **99,** 945–1485.

Montone, P., M. T. Mariucci, and S. Pierdominici (2012). The Italian present-day stress map, *Geophys. J. Int.* **189,** 705–716, doi: 10.1111/j.1365-246X.2012.05391.x.

Mucciarelli, M., M. Bianca, R. Ditommaso, M. R. Gallipoli, A. Masi, C. Milkereit, S. Parolai, M. Picozzi, and M. Vona (2011). Far field damage on RC buildings: The case study of Navelli during the L'Aquila (Italy) seismic sequence, *Bull. Earthq. Eng.* **9,** 263–283, doi: 10.1007/s10518-010-9201-y.

Oglesby, D. D., R. J. Archuleta, and S. B. Nielsen (2000a). The dynamics of dip-slip faults: Explorations in two dimensions, *J. Geophys. Res.* **105,** 13,643–13,653.

Oglesby, D. D., R. J. Archuleta, and S. B. Nielsen (2000b). The three dimensional dynamics of dipping faults, *Bull. Seismol. Soc. Am.* **90,** 616–628.

Piccinini, D., N. A. Pino, and G. Saccorotti (2012). Source complexity of the May 20, 2012, M_w 5.9, Ferrara (Italy) event, *Ann. Geophys.* **55,** no. 4, 569–573, doi: 10.4401/ag-6111.

Pondrelli, S., S. Salimbeni, P. Perfetti, and P. Danecek (2012). Quick regional centroid moment tensor solutions for the Emilia 2012 (northern Italy) seismic sequence, *Ann. Geophys.* **55,** no. 4, doi: 10.4401/ag-6146.

Priolo, E., M. Romanelli, C. Barnaba, M. Mucciarelli, G. Laurenzano, L. Dall'Olio, N. Abu-Zeid, R. Caputo, G. Santarato, L. Vignola, C. Lizza, and P. Di Bartolomeo (2012). The Ferrara thrust earthquakes of May–June 2012: Preliminary site response analysis at the sites of the OGS temporary network, *Ann. Geophys.* **55,** no. 4, doi: 10.4401/ag-6172.

Rovida, A., R. Camassi, P. Gasperini, and M. Stucchi (Editors) (2011). CPTI11, the 2011 version of the Parametric Catalogue of Italian Earthquakes, Milano, Bologna, available at http://emidius.mi.ingv.it/CPTI/ (last accessed September 2013).

Salvi, S., C. Tolomei, J. P. Merryman Boncori, G. Pezzo, S. Atzori, A. Antonioli, E. Trasatti, R. Giuliani, S. Zoffoli, and A. Coletta (2012). Activation of the SIGRIS monitoring system for ground deformation mapping during the 2012 Emilia seismic sequence,

using COSMO-SkyMed InSAR data, *Ann. Geophys.* **55,** no. 4, doi: 10.4401/ag-6181.

Scognamiglio, L., L. Margheriti, F. M. Mele, E. Tinti, A. Bono, P. De Gori, V. Lauciani, F. P. Lucente, A. G. Mandiello, C. Marcocci, S. Mazza, S. Pintore, and M. Quintiliani (2012). The 2012 Pianura Padana Emiliana seismic sequence: Locations, moment tensors and magnitudes, *Ann. Geophys.* **55,** no. 4, doi: 10.4401/ag-6159.

Serpelloni, E., L. Anderlini, A. Avallone, V. Cannelli, A. Cavaliere, D. Cheloni, C. D'Ambrosio, E. D'Anastasio, A. Esposito, G. Pietrantonio, A. R. Pisani, M. Anzidei, G. Cecere, N. D'Agostino, S. Del Mese, R. Devoti, A. Galvani, A. Massucci, D. Melini, F. Riguzzi, G. Selvaggi, and V. Sepe (2012). GPS observations of coseismic deformation following the May 20 and 29, 2012, Emilia seismic events (northern Italy): Data, analysis and preliminary models, *Ann. Geophys.* **55,** no. 4, doi: 10.4401/ag-6168.

Tertulliani, A., L. Arcoraci, M. Berardi, F. Bernardini, B. Brizuela, C. Castellano, S. Del Mese, E. Ercolani, L. Graziani, A. Maramai, A. Rossi, M. Sbarra, and M. Vecchi (2012). The Emilia 2012 sequence: A macroseismic survey, *Ann. Geophys.* **55,** no. 4, doi: 10.4401/ag-6140.

Yang, F., Q. Luo, and W. Che (2010). Torsional phenomena in 2008 great Wenchuan earthquake, *Earthq. Sci.* **23,** 79–85, doi: 10.1007/s11589-009-0077-3.

Yegian, M. K., V. G. Ghahrman, and G. Gazetas (1994). Armenia Earthquake. II: Damage statistics versus geologic and soil profiles, *J. Geotech. Eng.* **120,** 21–45.

Luigi Cucci
Andrea Tertulliani
Istituto Nazionale di Geofisica e Vulcanologia
via di Vigna Murata 605
Roma, 00143 Italy
luigi.cucci@ingv.it
andrea.tertulliani@ingv.it